

Color, Flavor, Temperature and Magnetic Field Dependence of QCD Phase Diagram: Magnetic Catalysis and its Inverse

Aftab Ahmad,¹ Adnan Bashir,² Marco A. Bedolla,³ and J. J. Cobos-Martínez⁴

¹ *Institute of Physics and Electronics, Gomal University, 29220 D.I. Khan, K.P.K., Pakistan.*

² *Instituto de Física y Matemáticas, Universidad Michoacana de San Nicolás de Hidalgo, Edificio C-3, Ciudad Universitaria, C.P. 58040, Morelia, Michoacán, México.*

³ *Mesoamerican Centre for Theoretical Physics, Universidad Autónoma de Chiapas, Carretera Zapata Km. 4, Real del Bosque (Terán), Tuxtla Gutiérrez 29040, Chiapas, México.*

⁴ *Cátedra CONACyT, Departamento de Física, Centro de Investigación y de Estudios Avanzados del Instituto Politécnico Nacional, Apartado Postal 14-740, 07000, Ciudad de México, México.*

We study dynamical chiral symmetry breaking for quarks in the fundamental representation of $SU(N_c)$ for N_f number of light quark flavors. We also investigate the phase diagram of quantum chromodynamics at finite temperature T and/or in the presence of a constant external magnetic field eB . The unified formalism for this analysis is provided by a symmetry-preserving Schwinger-Dyson equations treatment of a vector \times vector contact interaction model which encodes several well-established features of quantum chromodynamics to mimic the latter as closely as possible. Deconfinement and chiral symmetry restoration are triggered above a critical value of N_f at $T = 0 = eB$. On the other hand, increasing temperature itself screens strong interactions, thus ensuring that a smaller value of N_f is sufficient to restore chiral symmetry at higher temperatures. We also observe the well-known phenomenon of magnetic catalysis for a strong enough magnetic field. However, we note that if the effective coupling strength of the model decreases as a function of magnetic field, it can trigger inverse magnetic catalysis in a certain window of this functional dependence. Our model allows for the simultaneous onset of dynamical chiral symmetry breaking and confinement for each case. Qualitative as well as quantitative predictions of our simple but effective model are in reasonably satisfactory agreement with lattice results and other reliable and refined predictions based upon intricate continuum studies of quantum chromodynamics.

PACS numbers: 11.10.Wx, 25.75.Nq, 98.62.En, 11.30.Rd, 11.30.Hv

I. INTRODUCTION

Quantum chromodynamics (QCD) is the theory of strong color force among quarks and gluons. Ultraviolet and infrared peculiarities of QCD hinge upon an interplay between the number of light quark flavors N_f and the number of colors N_c of the gauge group $SU(N_c)$. Sign of the one-loop β -function depends upon the factor $-11N_c + 2N_f$. In real life QCD, this sign is negative as $N_c = 3$ outmuscles N_f and hence the strong interactions are asymptotically free [1–3]. Only in a universe with $N_f > (11/2)N_c$, this effect will be reversed and asymptotic freedom will be lost. Infrared QCD is even more eerie. It exhibits emergent phenomena of dynamical chiral symmetry breaking (DCSB) and confinement which are inconceivable in any perturbative approach to QCD.

Modern lattice analyses appear to demonstrate that the restoration of a chirally symmetric phase takes place somewhere between $N_f \approx 8 - 12$ [4–8]. Continuum studies of QCD back these claims and confirm that the phenomena of confinement and DCSB also owe themselves to the intricate balance between N_f and N_c . For $N_c = 3$, if the number of flavors exceeds $N_f \approx 7 - 12$, quarks are deconfined and chiral symmetry is restored, see for example Refs. [9–14].

The infrared behavior of QCD is also affected in the presence of a heat bath. At low temperatures, the ob-

servable degrees of freedom continue to be color-singlet hadrons, whereas at high temperatures, the interaction gets increasingly screened and weak, causing a hadron's constituents to deconfine into a phase where the dominant degrees of freedom are the defining ingredients of perturbative QCD, namely, quarks and gluons. Increasing T also triggers the transition of quarks with large effective constituent-like masses to quarks with only current masses. Needless to say, a quantitative study of this behavior has been widely carried out in literature, see for example Refs. [15–23] for lattice QCD and Refs. [24–32] for works based upon continuum techniques of Schwinger-Dyson equations (SDEs).

It is also well known that in the presence of strong magnetic fields, it is possible to generate fermion masses for any value of the coupling strength. This phenomenon was first studied in quantum electrodynamics (QED) and was dubbed as magnetic catalysis, see for example [33–39]. This phenomenon owes itself to dimensional reduction. Nonperturbative aspects of dynamical mass generation in the presence of magnetic fields have also been studied in continuum QCD [40, 41], as well as lattice QCD [42].

QCD phase diagram has also been studied in the presence of external magnetic fields. It is observed that near the cross-over temperature, chiral quark condensate develops a peculiar behaviour. It starts decreasing with increasing magnetic field. This effect has come to be known as inverse magnetic catalysis (IMC), [43–47], or

magnetic inhibition, [48]. Continuum QCD studies support these findings, [49]. It is important to highlight that this effect is believed to be triggered both by the weakening of the running coupling and the gluon dynamics. Therefore, any model-building must incorporate important QCD features to stand any reasonable chance to capture the correct behavior of this theory at finite temperature in the presence of external magnetic fields. This is precisely what our contact interaction (CI) model does. It is designed to meet the following requirements:

1. It produces right amount of DCSB at $T = 0 = eB$. Consequently, it has extensively been applied to satisfactorily calculate static properties of light and heavy hadrons, [50–58].
2. It takes into account an infrared mass scale connected to the gluon mass which is known to emerge in non perturbative QCD, [59–63].
3. The color and light flavor dependence of DCSB and confinement are suitably built-in to mimic the recent QCD findings both on the lattice and in continuum QCD studies, [4–14].
4. It implements confinement by ensuring the absence of quark production thresholds.
5. It supports the phenomenon of magnetic catalysis at zero temperature and inverse magnetic catalysis at finite temperature [64]. We improve and generalize this model to study the dependence of these phenomena on the massless quark flavors. We require both the emergent phenomena of DCSB and confinement to be interlinked and simultaneous as evidence suggests [46, 49].

Equipped with a carefully constructed QCD based model under extreme conditions, we investigate its phase diagram as a function of colors N_c , light quark flavors N_f , finite temperature T and external magnetic field eB . All the predictions align satisfactorily with modern findings of the QCD phase diagram while avoiding computational complexities of lattice and refined continuum studies.

In Sec. II, we recall the quark gap equation, define the CI model and solve it as a function of N_c and N_f . For each N_c , there is a critical value of N_f above which chiral symmetry is restored. After the screening dynamics has been adequately incorporated into the CI, we study the QCD phase diagram in Sec. III and obtain the cross-over temperature for chiral symmetry restoration and deconfinement. Sec. IV is devoted to the same study with an external magnetic field replacing the thermal bath. We are able to describe magnetic catalysis with its known characteristics. In Sec. V, DCSB and confinement are studied as a function of external magnetic field, temperature and light quark flavors. We find IMC in a region including the cross-over temperature. Sec. VI provides conclusions and discussion.

II. THE GAP EQUATION

We start by presenting the generalities of the CI for the quark fields. In order to include the anti-screening effects of the gluons and the screening effects of the light quarks, we extend the model to an $SU(N_c)$ gauge theory with N_f number of light quarks.

A. The Contact Interaction

The dressed-quark propagator S is obtained by solving the quark SDE

$$S^{-1}(p) = i\gamma \cdot p + m_f + \int \frac{d^4 q}{(2\pi)^4} g^2 D_{\mu\nu}(p-q) \frac{\lambda^a}{2} \gamma_\mu S(q) \Gamma_\nu^a(p, q), \quad (1)$$

where m_f is the bare quark mass, g is the QCD coupling constant, λ^a are the Gell-Mann matrices, Γ_ν^a is the dressed quark-gluon vertex and $D_{\mu\nu}$ is the gluon propagator.

As we have mentioned before, in a series of previous articles, it has been shown that at zero temperature, the static properties of low-lying mesons and baryons can be faithfully reproduced by assuming that the quarks interact, not via massless vector-boson exchange, but instead through a symmetry preserving vector-vector CI with a finite gluon mass [50–57]:

$$g^2 D_{\mu\nu}(k) = \delta_{\mu\nu} \frac{4\pi\alpha_{\text{IR}}}{m_G^2} \equiv \delta_{\mu\nu} \alpha_{\text{eff}}, \quad (2)$$

$$\Gamma_\mu^a(p, q) = \frac{\lambda^a}{2} \gamma_\mu, \quad (3)$$

where $m_G = 500$ MeV is an infrared gluon mass scale which is generated dynamically in QCD [59–63, 65], and $\alpha_{\text{IR}} = 0.36\pi$ specifies the strength of the infrared interaction. There is a critical value of α_{eff} above which chiral symmetry is dynamically broken.

Eqs. (2) and (3) specify the kernel in the quark SDE, Eq. (1). In this approximation, the dressed-quark propagator takes a very simple form :

$$S^{-1}(p) = i\gamma \cdot p + M, \quad (4)$$

where M is momentum independent dynamical quark mass, to be determined from Eq. (1). If we substitute Eqs. (2,3,4) into Eq. (1), and recall that in the fundamental representation of $SU(N_c)$, the Gell-Mann matrices satisfy the identity $\sum_{a=1}^8 \lambda^a \lambda^a = 2(N_c - 1/N_c)$, we get

$$M = m_f + \frac{\alpha_{\text{eff}}^{N_c}(N_f)M}{8\pi^2} \int_0^\infty ds \frac{s}{s + M^2}, \quad (5)$$

where

$$\alpha_{\text{eff}}^{N_c}(N_f) = (N_c - 1/N_c) \alpha_{\text{eff}}(N_f). \quad (6)$$

Since the integral in Eq. (5) is divergent, we must adopt a regularization procedure. After exponentiation of the denominator of the integrand and employing the confining proper-time regularization [66], we can write

$$\frac{1}{s+M^2} = \int_0^\infty d\tau e^{-\tau(s+M^2)} \rightarrow \int_{\tau_{UV}^2}^{\tau_{IR}^2} d\tau e^{-\tau(s+M^2)} = \frac{e^{-\tau_{UV}^2(s+M^2)} - e^{-\tau_{IR}^2(s+M^2)}}{s+M^2}. \quad (7)$$

Here, $\tau_{IR,UV}^{-1} = \Lambda_{IR,UV}$ are infra-red and ultra-violet regulators, respectively. A non-zero value for τ_{IR} implements confinement by ensuring the absence of quarks production thresholds [67]. It has been shown that an excitation described by a pole-less propagator would never reach its mass-shell [66]. Moreover, since Eq. (2) does not define a renormalizable theory, Λ_{UV} cannot be removed, but instead plays a dynamical role, setting the scale for all dimensioned quantities. After integration over s , the gap equation reads :

$$M = m_f + \frac{\alpha_{\text{eff}}^{N_c}(N_f)}{8\pi^2} M \int_{\tau_{UV}^2}^{\tau_{IR}^2} d\tau \tau^{-2} e^{-\tau M^2}. \quad (8)$$

We shall use the notation $\alpha_{\text{eff}}^{N_c}(N_f) = \alpha_{\text{eff}}(N_f)$ for $N_c = 3$. Moreover, $\alpha_{\text{eff}}(N_f) = \alpha_{\text{eff}}$ for $N_f = 2$. We employ the parameters of Ref. [53], namely, we fix the coupling to:

$$\alpha_{\text{eff}} = 5.7 \times 10^{-5} \text{ MeV}^{-2}, \quad (9)$$

and use the following infrared and ultraviolet cutoffs:

$$\tau_{IR} = (240 \text{ MeV})^{-1}, \quad \tau_{UV} = (905 \text{ MeV})^{-1}. \quad (10)$$

These parameters have been fitted to the value of the chiral quark condensate in the vacuum. Along with $m_f = 0$, we obtain $M = 358 \text{ MeV}$ and $\langle \bar{u}u \rangle^{1/3} = \langle \bar{d}d \rangle^{1/3} = -241 \text{ MeV}$ for the dynamical mass of the u/d quarks and the chiral quark condensate for two quark flavors ($N_f = 2$, $N_c = 3$), respectively.

B. Colors, flavors and chiral symmetry breaking

To study the effect of light quark flavors N_f on the DCSB, we adopt the following flavor-dependence of the effective coupling:

$$\alpha_{\text{eff}}^{N_c}(N_f) = \alpha_{\text{eff}}^{N_c} \sqrt{1 - \frac{(N_f - 2)}{\lambda}}. \quad (11)$$

This form owes itself to the pattern of DCSB as observed in [11]. The dynamical quark mass in that work was observed to be $m_{\text{dyn}} \sim \sqrt{1 - N_f/N_f^c}$ where N_f^c is the critical number of flavors above which chiral symmetry is restored (see Eq. (8) of that article). Only a similar square root dependence in the coupling, Eq. (11), leads to this observed behavior. Thus the functional form in

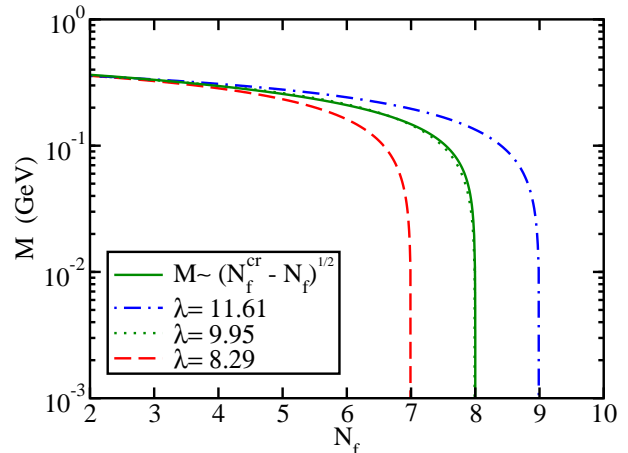


FIG. 1: Dynamical quark mass in the chiral limit as a function of flavors N_f with $N_c = 3$ for three different values of λ which ensures dynamical mass vanishes at $N_f^{\text{cr}} = 7, 8$ and 9 .

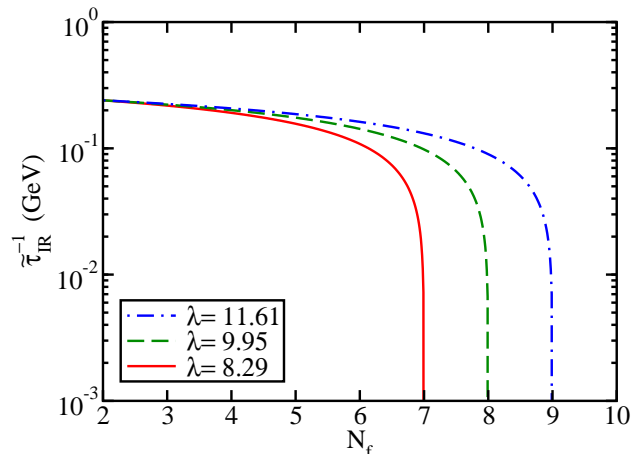


FIG. 2: Confining length scale in the chiral limit as a function of N_f flavors with $N_c = 3$ colors. The critical number of flavors for confinement are $N_f^{\text{cr}} = 7, 8$ and 9 .

Eq. (11) can be traced back to the flavor dependence of the gluon propagator in QCD, [63]. Due to this direct connection, note that $\lambda \sim N_f^c + \delta$, where $\delta \sim 1.2 - 2.6$ for the cases of interest to us. The appearance of δ is due to the factor $N_f - 2$ in Eq. (11).

Employing this coupling, we solve the gap equation, Eq. (8). For $N_c = 3$, we identify different values of λ to obtain critical values of N_f ($N_f^{\text{cr}} = 7, 8, 9$) above which the screening effects restore chiral symmetry. These numbers are in accordance with the findings of Ref. [11], later

reproduced in [14].

In Fig. 1, we display the variation of the dynamical mass M as a function of the number of flavors N_f . We compare one of the plots with a fit given by $M \sim \sqrt{N_f^{cr} - N_f}$, see [11], for $N_f^{cr} = 8$. It corresponds to $\lambda = 9.95$. The numerical results are very well described by this analytic form, reaffirming that our CI model mimics the refined continuum studies presented in [11]. For the remainder of the article, we choose the parameters to reproduce $N_f^{cr} = 8$ unless otherwise mentioned.

Recall that the confinement parameter is τ_{IR} . Simultaneous DCSB and confinement can be readily incorporated into the model if we define a flavor dependent infrared cutoff :

$$\tilde{\tau}_{\text{IR}} = \tau_{\text{IR}} \frac{M(2)}{M(N_f)}, \quad (12)$$

where $M(2)$ is the dynamical mass when $N_f = 2$ and $N_c = 3$. In Eq. (12), $M(N_f) \rightarrow 0$, implies $\tilde{\tau}_{\text{IR}} \rightarrow \infty$ and hence quarks get deconfined in this model. Seen in conjunction with Fig. 1, plots in Fig. 2 provide a confirmatory numerical check that DCSB and confinement are simultaneous in our CI model.

As emphasized earlier, the number of quark colors N_c anti-screens the interactions while N_f screens them. This can be readily confirmed by plotting the dressed quark mass M for different number of flavors, see Fig. 3. For $N_f = 0$ the minimum value of N_c required to trigger DCSB is $N_c^{cr} \simeq 2$. As the number of massless quark flavors increases, mellowing down the interaction strength, higher color group $SU(N_c)$ has to be invoked to set off DCSB. This interplay, reminiscent of the asymptotic freedom, is depicted in Figs. 3, 4, 5.

III. DCSB AT FINITE TEMPERATURE T

At finite temperature, within the imaginary time formalism, we split the fermion four-momentum according to $q = (\omega_n, \vec{q})$, where $\omega_n = (2n+1)\pi T$ are the well-known fermionic Matsubara frequencies. We adopt the standard convention for momentum integration, namely:

$$\int \frac{d^4 q}{(2\pi)^4} \rightarrow T \sum_{n=-\infty}^{\infty} \int \frac{d^3 q}{(2\pi)^3}. \quad (13)$$

Thus, the gap equation in the chiral limit at finite temperature can be written as (for $N_c = 3$):

$$M = \frac{8\alpha_{\text{eff}}(N_f)MT}{3\pi^2} \sum_{n=-\infty}^{\infty} \int_0^{\infty} dq \frac{\vec{q}^2}{\vec{q}^2 + \omega_n^2 + M^2}. \quad (14)$$

This equation and some of its variants have been discussed in several works [64, 68–70]. To implement proper time regularization, we exponentiate the denominator for

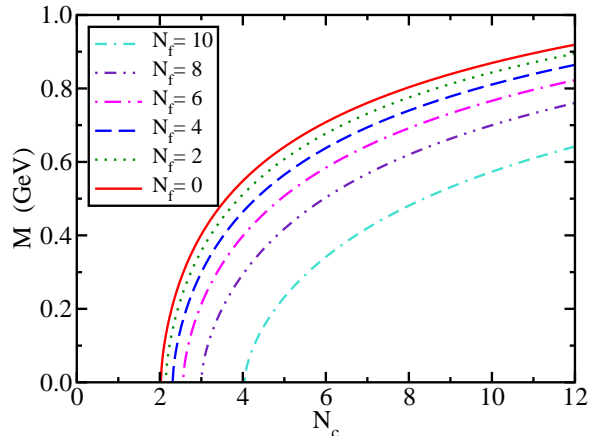


FIG. 3: Dynamical mass in the chiral limit as a function of N_c for different values of N_f . With increasing N_f , higher N_c is required to trigger DCSB. For $N_f = 0$, the dynamical mass vanishes below $N_c^{cr} \approx 2$.

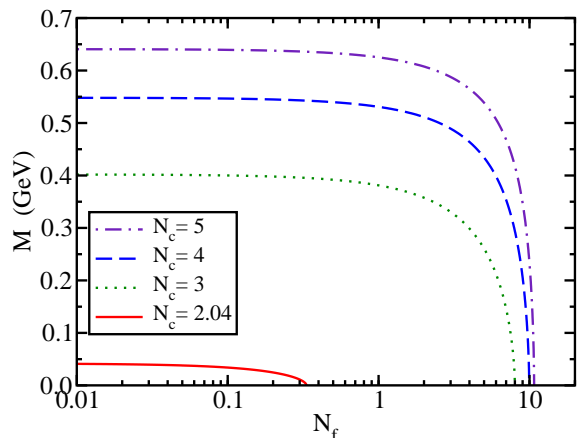


FIG. 4: Dynamical mass in the chiral limit as a function of quark flavors for several values of N_c . For a given N_c , one can increase N_f to a critical value such that the interaction strength diminishes enough to suppress DCSB.

each ω_n as follows :

$$\frac{1}{\vec{q}^2 + \omega_n^2 + M^2} \rightarrow \int_{\tau_{\text{UV}}^2}^{\tau_{\text{IR}}^2} d\tau e^{-\tau(\vec{q}^2 + \omega_n^2 + M^2)}, \quad (15)$$

with

$$\tilde{\tau}_{\text{IR}} = \tau_{\text{IR}} \frac{M(0, 2)}{M(T, N_f)}, \quad (16)$$

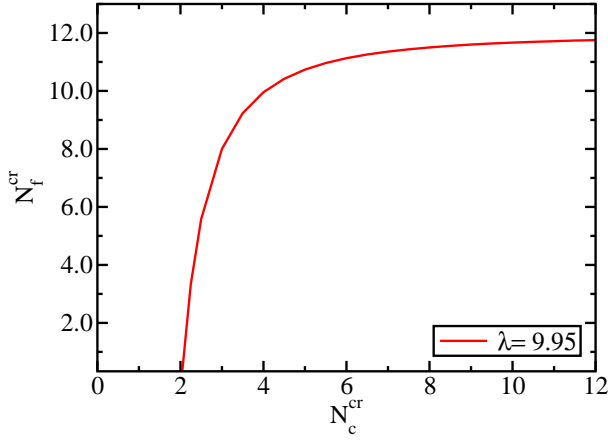


FIG. 5: Critical number of flavors N_f^{cr} as a function of critical number of colors N_c^{cr} . The above figure demonstrates the diametrically opposed effects of these two parameters.

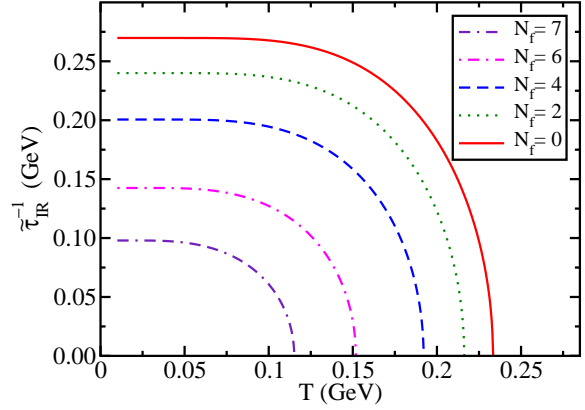


FIG. 7: Confining length scale as a function of T for different values of N_f . Its behavior is very similar to the DCSB. Increasing temperature of the heat bath eventually restores chiral symmetry.

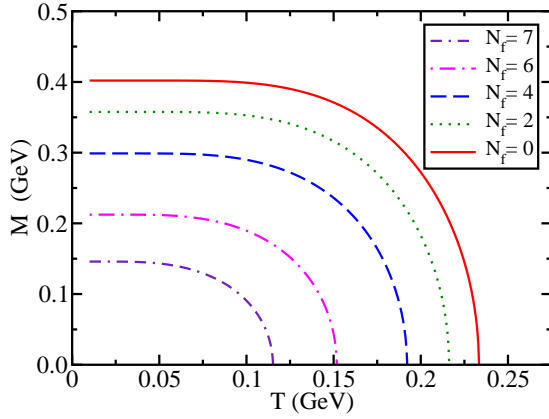


FIG. 6: Dynamical mass as a function of T for different number of flavors N_f . For $N_f \geq 8$ there is no generated mass.

where $M(0, 2)$ is the dynamical mass at $T = 0$, $N_f = 2$ and $N_c = 3$. Thus, in the chiral limit, the confining scale vanishes at the chiral symmetry restoration temperature. This is a simple way of ensuring the coincidence of transitions to confinement and DCSB phase. Summation over Matsubara frequencies and the remaining radial integration are carried out by using the following identities:

$$\sum_{n=-\infty}^{\infty} e^{-\tau \omega_n^2} = \Theta_2(0, e^{-(2\pi T)^2 \tau}), \quad (17)$$

$$\int_0^{\infty} dq \bar{q}^2 e^{-\tau \bar{q}^2} = \frac{\sqrt{\pi}}{4\tau^{3/2}}, \quad (18)$$

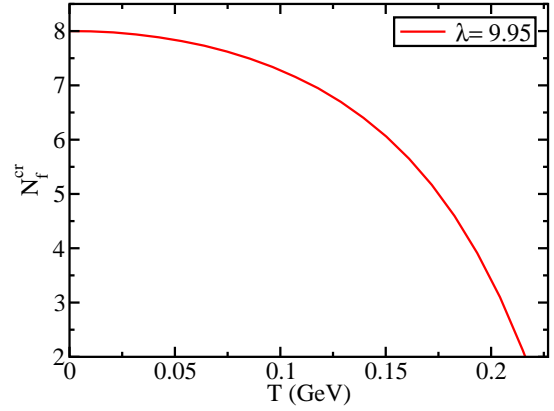


FIG. 8: The phase diagram of chiral symmetry and confinement for N_f^{cr} vs $T = T_c$. The N_f^{cr} and T_c are obtained from the thermal gradient of the dynamical mass $\partial_T M$ and of the confining scale, i.e., $\partial_T \tilde{\tau}_{\text{IR}}^{-1}$.

where $\Theta_2(x, y)$ represents the second Jacobi theta function. Finally, we arrive at the expression for the gap equation at finite temperature :

$$M = \frac{2\alpha_{\text{eff}}(N_f)MT}{3\pi^{3/2}} \int_{\tau_{\text{UV}}^2}^{\tau_{\text{IR}}^2} d\tau \frac{e^{-M^2 \tau} \Theta_2(0, e^{-(2\pi T)^2 \tau})}{\tau^{3/2}}. \quad (19)$$

In this chiral limit, the thermal evolution of dynamical mass M , for different values of N_f , is shown in Fig. 6. As expected, with increasing temperature, the strong interaction gets weakened, and, therefore, a lower value for

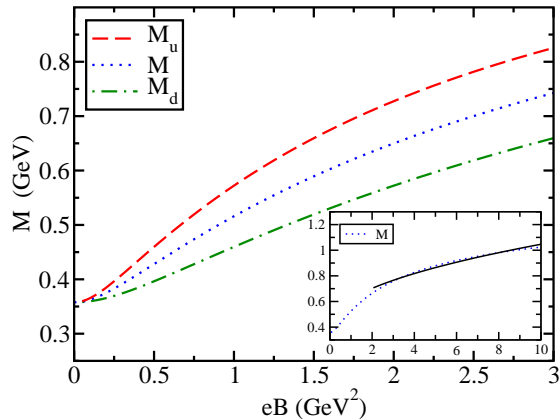


FIG. 9: Dynamical mass in the chiral limit for u ($Q_u = +2e/3$), d ($Q_d = -e/3$) quarks as a function of the strength of the magnetic field, for $N_f = 2$ and $N_c = 3$. M denotes the average dynamical mass, Eq. (25), obtained by solving its gap equation, Eq. (25)

the critical number of massless quark flavors is needed to restore chiral symmetry for a given value of N_c (3 in this case). A similar behavior is expected and observed for the confinement scale $\tilde{\tau}_{\text{IR}}^{-1}$, see Fig. 7. Unlike the competing forces of N_c and N_f , temperature T and the number of flavors N_f both catalyze chiral symmetry restoration and deconfinement. Note that the temperatures for the chiral symmetry breaking-restoration (T_c^x), confinement-deconfinement transitions (T_c^c) as a function of N_f^{cr} , shown in Fig. 8, are determined, respectively, from the position of the divergences of their thermal gradients $\partial_T M$ and $\partial_T \tilde{\tau}_{\text{IR}}^{-1}$. The model construction ensures these critical temperatures are coincidental, $T_c^x = T_c^c \equiv T_c \simeq 216.5$ MeV for $N_f = 2$ and $N_c = 3$ [64, 68, 70].

In the following section, instead of a thermal bath, we study the effect of a constant and uniform external magnetic field on the DCSB and confinement within this framework of the CI.

IV. GAP EQUATION IN A MAGNETIC FIELD WITH $N_c = 3$

In this section we consider a background homogeneous magnetic field directed along the z -axis, with magnitude B and defined through the symmetric gauge vector potential:

$$A_\mu^{ext} = \left(0, -\frac{By}{2}, \frac{Bx}{2}, 0\right). \quad (20)$$

The quark propagator $S(q)$ gets dressed with magnetic field effects, $S(q) \rightarrow \tilde{S}(q)$, in the Fock-Schwinger repre-

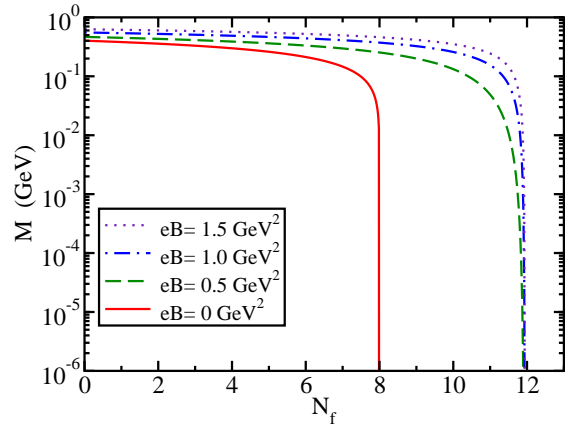


FIG. 10: Dynamical average mass M as a function of N_f and magnetic field strength eB in the chiral limit for $N_c = 3$.

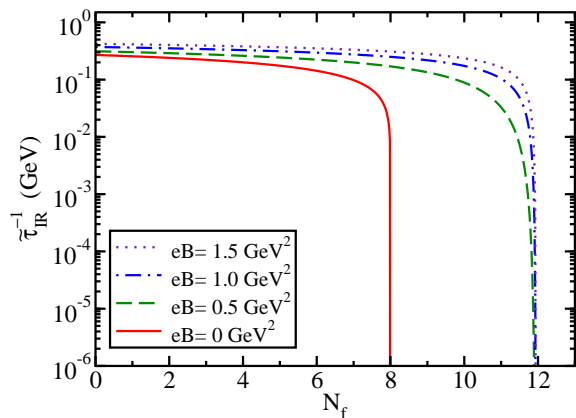


FIG. 11: Confining length scale as a function of N_f and magnetic field strength eB in the chiral limit for $N_c = 3$.

sentation [71, 72], and it is:

$$\begin{aligned} \tilde{S}(q) = & \int_0^\infty ds \frac{e^{-s(q_\parallel^2 + q_\perp^2 \frac{\tan(|Q_t B s|)}{|Q_t B s|} + M^2)}}{\cosh(|Q_t B s|)} \\ & \times \left[\left(\cosh(|Q_t B s|) - i\gamma^1 \gamma^2 \sinh(|Q_t B s|) \right) \right. \\ & \left. \times \left(M - \not{q}_\parallel \right) - \frac{\not{q}_\perp}{\cosh(|Q_t B s|)} \right], \quad (21) \end{aligned}$$

where the parallel and transverse splitting of quark momenta is in reference to the magnetic field direction, as

usual¹, and \mathcal{Q}_l ($\mathcal{Q}_u = +2e/3$, $\mathcal{Q}_d = -e/3$) refers to the electric charge of the light quarks, with $l = u, d$. With these ingredients, we adopt the regularization procedure from the previous section. The corresponding gap equation for the dynamical mass at zero temperature under the influence of a uniform magnetic field for the light quarks becomes:

$$M_l = \frac{16\alpha_{\text{eff}}(N_f)}{3} M_l \int \frac{d^2 q_\perp}{(2\pi)^2} \frac{d^2 q_\parallel}{(2\pi)^2} \times \int_{\tau_{\text{UV}}^2}^{\tau_{\text{IR}}^2} d\tau e^{-\tau(q_\parallel^2 + q_\perp^2 \frac{\tanh(|\mathcal{Q}_l B \tau|)}{|\mathcal{Q}_l B \tau|} + M_l^2)}. \quad (22)$$

On using the relations:

$$\int \frac{d^2 q_\parallel}{(2\pi)^2} e^{-\tau q_\parallel^2} = \frac{1}{4\pi\tau},$$

$$\int \frac{d^2 q_\perp}{(2\pi)^2} e^{-\tau q_\perp^2 \frac{\tanh(|\mathcal{Q}_l B \tau|)}{|\mathcal{Q}_l B \tau|}} = \frac{|\mathcal{Q}_l B|}{4\pi \tanh(|\mathcal{Q}_l B \tau|)}, \quad (23)$$

we obtain the gap equation for massless quarks at zero temperature in an external magnetic field

$$M_l = \frac{\alpha_{\text{eff}}(N_f)}{3\pi^2} |\mathcal{Q}_l B| \int_{\tau_{\text{UV}}^2}^{\tau_{\text{IR}}^2} d\tau \frac{M_l e^{-M_l^2 \tau}}{\tau \tanh(|\mathcal{Q}_l B \tau|)}, \quad (24)$$

where $l = u, d$. In Fig. 9, we show numerical results for the dynamical mass of the u and d quarks in the chiral limit as a function of eB . The so-called magnetic catalysis effect is clearly seen in this figure, and its influence is bigger in the case of the u quark due to its larger charge, compared to the d quark.

For our purposes, and in order to make the analysis flavor-independent, in the following we will work with the average dynamical mass in the chiral limit,

$$M = \frac{1}{2}(M_u + M_d), \quad (25)$$

whose gap equation is given by

$$M = \frac{\alpha_{\text{eff}}(N_f)}{3\pi^2} \frac{1}{2} \sum_{l=u,d} |\mathcal{Q}_l B| \int_{\tau_{\text{UV}}^2}^{\tau_{\text{IR}}^2} d\tau \frac{M e^{-M^2 \tau}}{\tau \tanh(|\mathcal{Q}_l B \tau|)}. \quad (26)$$

In Fig. 9, we show numerical results for the average dynamical quark mass in the chiral limit as a function of eB (dotted line). In the inset of Fig. 9, we plot again the average dynamical quark mass in the chiral limit as a function of eB , but this time for eB up to $eB = 10 \text{ GeV}^2$. We note that for large values of eB , the dependence of M on eB , is given by \sqrt{eB} ; see the continuous line in the inset of Fig. 9.

In Fig. 10, we present the evolution of dynamical average mass M as a function of the number of flavors N_f

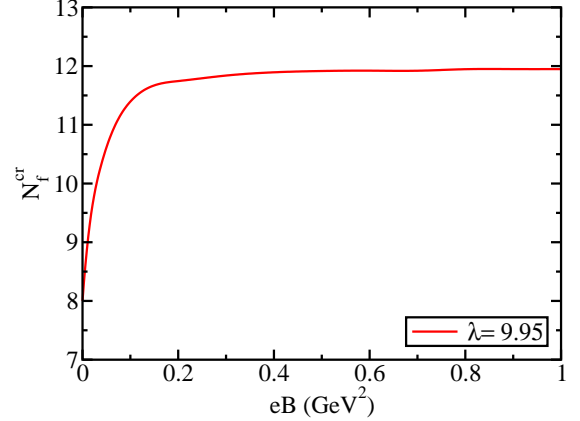


FIG. 12: The phase diagram of chiral symmetry and confinement for N_f^{cr} vs eB . N_f^{cr} is obtained from the magnetic gradient of the chiral condensate $\partial_{eB} \langle \bar{\psi} \psi \rangle^{1/3} (N_f, eB)$ and of the confining scale $\partial_{eB} \tilde{\tau}_{\text{IR}}^{-1} (N_f, eB)$.

for various values of the magnetic field eB . In this plot, we see that the value of eB , whose magnetic catalysis enhances DCSB, competes against N_f to generate dynamical mass. On the other hand, Fig. 11 shows the behavior of the confinement scale as a function of N_f . From both figures, we can see that increasing eB tends to increase the N_f^{cr} needed for chiral symmetry restoration, contrary to the behavior of the critical number of fermions N_f^{cr} as a function of temperature where it gets reduced as T is increased (see Fig. 8).

That effect is clearer in Fig. 12, where we show the evolution of critical N_f^{cr} with respect to eB . These critical values are obtained by locating the position of the divergences of their magnetic gradients $\partial_{eB} M$ and $\partial_{eB} \tilde{\tau}_{\text{IR}}^{-1}$.

V. PHASE DIAGRAM AT FINITE T AND B

At finite temperature T and in a magnetic field eB , the gap equation beyond the chiral limit reads:

$$M_l = m + \frac{16\alpha_{\text{eff}}(N_f)}{3} M_l T \sum_{n=-\infty}^{\infty} \int \frac{dq_3}{(2\pi)} \frac{d^2 q_\perp}{(2\pi)^2} \times \int_{\tau_{\text{UV}}^2}^{\tau_{\text{IR}}^2} d\tau e^{-\tau(\omega_n^2 + q_3^2 + q_\perp^2 \frac{\tanh(|\mathcal{Q}_l B \tau|)}{|\mathcal{Q}_l B \tau|} + M_l^2)}, \quad (27)$$

for quark flavor $l = u, d$. We work for the isospin symmetric case, taking $m_u = m_d = m = 7 \text{ MeV}$. After performing the sum over Matsubara frequencies, integrating over q_3 and q_\perp , the gap equation of the average mass,

¹ Recall that $q^2 = q_\parallel^2 + q_\perp^2$, with $q_\parallel^2 = q_0^2 + q_3^2$ and $q_\perp^2 = q_1^2 + q_2^2$.

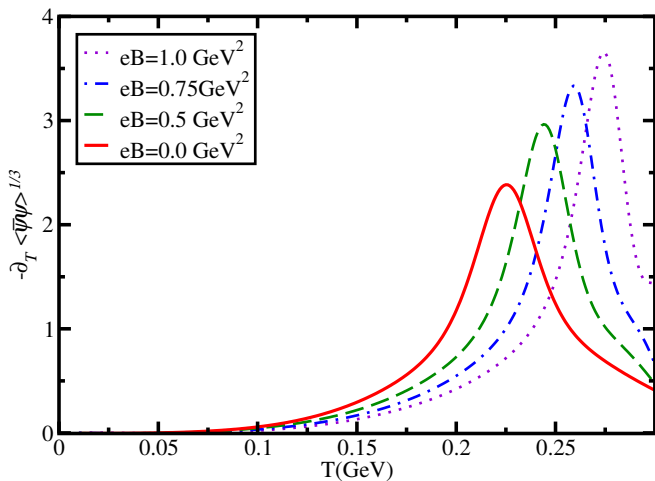


FIG. 13: The thermal gradient of the chiral condensate $\partial_T \langle \bar{\psi}\psi \rangle^{1/3} (N_f = 2, eB, T)$ has been plotted as a function of T for various values of eB using the magnetic field independent coupling. It displays the usual feature of magnetic catalysis. For higher T , chiral symmetry breaking is triggered at larger values of eB .

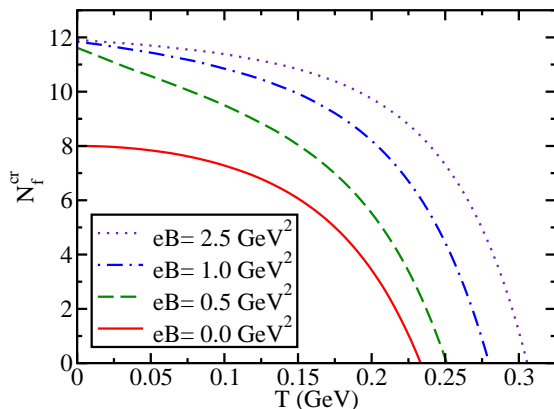


FIG. 14: The phase diagram of chiral symmetry and confinement in the N_f^{cr} vs T_c for various values of eB . The N_f^{cr} is obtained from the thermal gradient of the chiral condensate $\partial_T \langle \bar{\psi}\psi \rangle^{1/3} (N_f, eB, T)$ and of the confining scale $\partial_T \tilde{\tau}_{\text{IR}}^{-1} (N_f, eB, T)$.

Eq. (25), at finite temperature and magnetic field is:

$$M = m + \frac{2\alpha_{\text{eff}}(N_f)MT}{3\pi^{3/2}} \frac{1}{2} \sum_{l=u,d} |Q_l B| \times \int_{\tau_{\text{UV}}^2}^{\tau_{\text{IR}}^2} d\tau \frac{e^{-M^2\tau} \Theta_2(0, e^{-(2\pi T)^2\tau})}{\tau^{1/2} \tanh(|Q_l B|\tau)}, \quad (28)$$

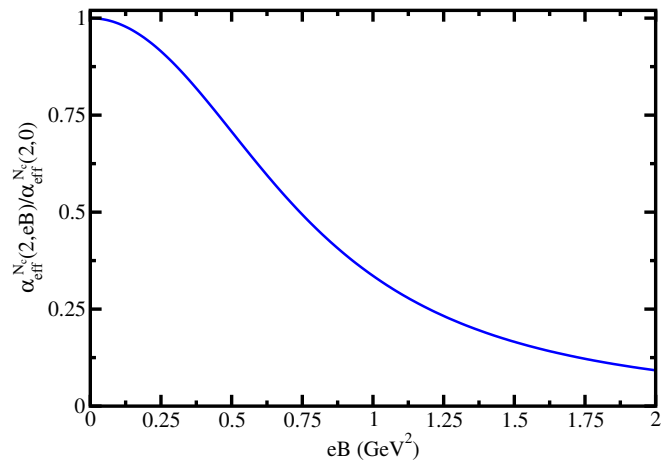


FIG. 15: Magnetic field dependent coupling of Eq. (30).

where

$$\tilde{\tau}_{\text{IR}} = \tau_{\text{IR}} \frac{M(0, 0, 2)}{M(T, eB, N_f)}. \quad (29)$$

The thermal gradient of the dynamical mass whose maximum points to the onslaught of DCSB has been plotted as a function of temperature for varying magnetic field in Fig 13. We observe a typical pattern of magnetic catalysis. Increasing temperature requires larger magnetic field to catalyze DCSB.

In Fig. 14, we plot N_f^{cr} as a function of temperature for different values of the magnetic field. We see the expected interplay between the magnetic field and the temperature: the greater the value of magnetic field, the higher is the temperature required to restore chiral symmetry. For any given value of the magnetic field strength, the critical value of the number of massless quark flavors decreases with the (critical) temperature just as in the absence of the external magnetic field. This pattern is again along the lines of the common wisdom of magnetic catalysis. The only difference now is that the required N_f^{cr} is somewhat larger for higher values of the magnetic field.

It is well known that the effect of the magnetic field must be taken into account in the functional dependence of the interaction strength. If α_s decreases with increasing eB in a certain range of values of the magnetic field, it suppresses the formation of chiral quark condensate. This is what produces IMC. In order to incorporate the magnetic field dependence in the coupling constant and study its effect on N_f^{cr} , we follow [64, 73] and adopt the following Padé approximant for the eB -dependent interaction strength

$$\alpha_{\text{eff}}^{N_c}(N_f, x) = \alpha_{\text{eff}}^{N_c}(N_f, 0) \left(\frac{1 + ax^2 + bx^3}{1 + cx^2 + dx^4} \right), \quad (30)$$

where the N_f dependence of the coupling, $\alpha_{\text{eff}}^{N_c}(N_f, 0)$, is given by Eq. (11), $x = eB/\Lambda_{\text{QCD}}^2$, with $\Lambda_{\text{QCD}} = 300$

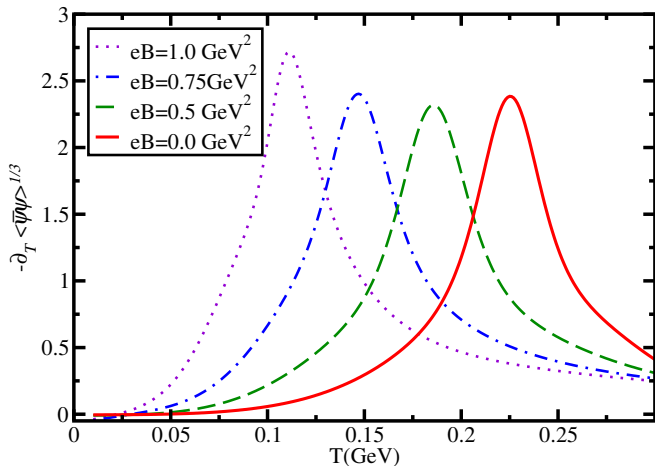


FIG. 16: The thermal gradient of the chiral condensate $\partial_T \langle \bar{\psi}\psi \rangle^{1/3} (N_f = 2, eB, T)$ has been plotted as a function of T for various values of eB using the magnetic field dependent coupling of Eq. (30). It now exhibits IMC. For higher T , chiral symmetry breaking occurs at lower values of eB .

MeV. The parameters a, b, c and d were obtained [73] through reproducing the critical transition temperature for chiral transition for different values of the magnetic field strength, obtained by lattice QCD [44]. The modified coupling is shown in Fig. 15. We have refrained from avoiding any additional N_f dependence in this modified coupling. We have no theoretical or phenomenological indications about the existence, let alone the the nature of such correlations between N_f and eB -dependence.

In Fig. 16, we redo the plot of thermal gradient of the dynamical mass against temperature. We now observe a diametrically opposed behavior. Increasing temperature requires lower magnetic field for the onslaught of DCSB. This is the well known IMC.

In Fig. 17, we plot the new $N_f - T$ phase diagram for varying magnetic field. As can be readily inferred from this figure, the behaviour of the curves N_f^{cr} , as a function of T , is opposite to that found in Fig. 13. This is another manifestation of the IMC phenomenon predicted in this CI effective model. Lower values of eB demand higher N_f^{cr} against the conventional wisdom of magnetic catalysis. Note that IMC is not seen when temperatures are sufficiently low as compared to the cross-over region.

We can certainly do better than Eq. (30). The running coupling must also be a function of temperature. This refined approach was adopted in [74, 75]. We follow [74], adopt their parameters and define

$$\alpha_{\text{eff}}^{N_c}(N_f, x, y) = \alpha_{\text{eff}}^{N_c}(N_f, 0, 0) \frac{1 - \gamma xy}{1 + \alpha \ln(1 + \beta x)}, \quad (31)$$

where $y = T/\Lambda_{\text{QCD}}$. The parameters α and β are fixed to obtain a reasonable description of the lattice average of up and down quark condensates at $T = 0$. γ is obtained from a similar fit at the highest temperatures. We now

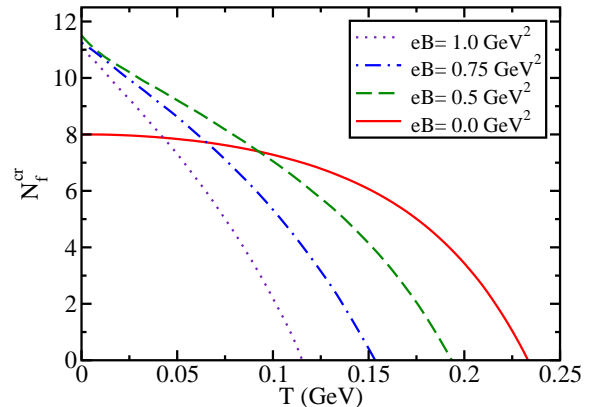


FIG. 17: The phase diagram of chiral symmetry and confinement for N_f^{cr} vs T_c at finite eB obtained with an eB -dependent coupling of Eq. (30). The N_f^{cr} is obtained from the thermal gradient of the chiral condensate $\partial_T \langle \bar{\psi}\psi \rangle^{1/3} (N_f, eB, T)$ and of the confining scale $\partial_T \tilde{\tau}_{\text{IR}}^{-1} (N_f, eB, T)$

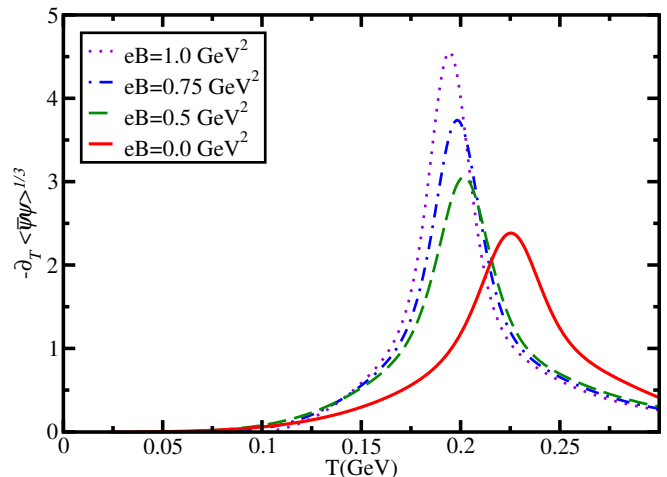


FIG. 18: The thermal gradient of the chiral condensate $\partial_T \langle \bar{\psi}\psi \rangle^{1/3} (N_f = 2, eB, T)$ has been plotted as a function of T for various values of eB using the magnetic field and temperature dependent coupling of Eq. (31). It again exhibits IMC.

employ this coupling to show the corresponding plots in Fig. 18 and Fig. 19. Note that the IMC persists but in a narrower window near the cross-over temperature.

VI. DISCUSSION AND CONCLUSIONS

We incorporate flavor dependence in our CI model to mimic the latest SDE and lattice results. These

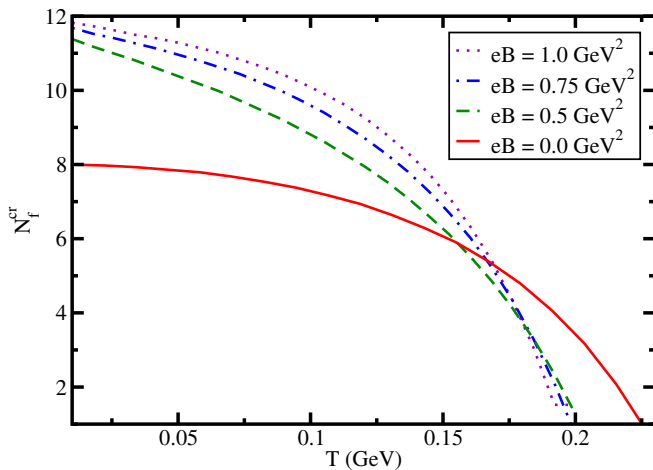


FIG. 19: The phase diagram of chiral symmetry and confinement for N_f^{cr} vs T_c at finite eB obtained now with an (eB, T) -dependent coupling of Eq. (31).

results show that chiral symmetry is restored and deconfinement is triggered above $N_f \approx 7 - 10$, [9–14]. This observation is in accordance with the expectation that increasing light quark flavors screen the interaction in contrast with the anti-screening effect of colors. For $N_f = 2$ (corresponding to u and d flavors), we find that the interaction is strong enough to break chiral symmetry only above $N_c \approx 2.2$. The nearest such integer is 3 which corresponds to the observed reality.

Additionally, the critical value N_f^{cr} decreases inversely with temperature. Temperature itself screens QCD in-

teractions, thus ensuring even a small value of N_f is sufficient to switch off DCSB.

Similarly, the presence of an external magnetic field also influences the value of N_f^{cr} . N_f^{cr} grows with the increase of magnetic field as higher values of the later make it increasingly harder to pull the plug on chiral symmetry breaking.

Last but not least, we explore the phase diagram for simultaneous variation of temperature and external magnetic field. We observe the usual magnetic catalysis for a strong enough magnetic field if the coupling strength is independent of the field. However, if we incorporate effective coupling of the model which decreases as a function of magnetic field in accordance with lattice studies, it triggers IMC in our model just as most modern studies suggest. To the best of our knowledge, this work, for the first time, knits the quark flavor dependence with that of temperature and magnetic field in accordance with the current theoretical and phenomenological understanding of this field of study. We plan to investigate hadronic bound states within this model in future.

VII. ACKNOWLEDGEMENTS

We acknowledge financial support by CONACyT and CIC-UMSNH, Mexico, with research Grant Nos. CB-2014-242117 and 4.10, respectively. We thank G. Krein and J. Rodríguez-Quintero for their helpful comments on the draft version of this article. A. Ahmad thanks A. Raya and P. Rioseco for their hospitality during his stay at the IFM, UMSNH, Mexico.

-
- [1] D. J. Gross and F. Wilczek, Phys. Rev. Lett. **30**, 1343 (1973). doi:10.1103/PhysRevLett.30.1343
- [2] H. D. Politzer, Phys. Rev. Lett. **30**, 1346 (1973). doi:10.1103/PhysRevLett.30.1346
- [3] D. J. Gross and F. Wilczek, Phys. Rev. D **8**, 3633 (1973). doi:10.1103/PhysRevD.8.3633
- [4] M. Hayakawa, K.-I. Ishikawa, Y. Osaki, S. Takeda, S. Uno and N. Yamada, Phys. Rev. D **83**, 074509 (2011) doi:10.1103/PhysRevD.83.074509 [arXiv:1011.2577 [hep-lat]].
- [5] A. Cheng, A. Hasenfratz, G. Petropoulos and D. Schaich, JHEP **1307**, 061 (2013) doi:10.1007/JHEP07(2013)061 [arXiv:1301.1355 [hep-lat]].
- [6] T. Appelquist *et al.* [LSD Collaboration], Phys. Rev. D **90**, no. 11, 114502 (2014) doi:10.1103/PhysRevD.90.114502 [arXiv:1405.4752 [hep-lat]].
- [7] A. Hasenfratz and D. Schaich, JHEP **1802**, 132 (2018) doi:10.1007/JHEP02(2018)132 [arXiv:1610.10004 [hep-lat]].
- [8] T. Appelquist *et al.* [Lattice Strong Dynamics Collaboration], Phys. Rev. D **99**, no. 1, 014509 (2019) doi:10.1103/PhysRevD.99.014509 [arXiv:1807.08411 [hep-lat]].
- [9] T. Appelquist, J. Terning and L. C. R. Wijewardhana, Phys. Rev. Lett. **77**, 1214 (1996) doi:10.1103/PhysRevLett.77.1214 [hep-ph/9602385].
- [10] T. Appelquist, A. G. Cohen and M. Schmaltz, Phys. Rev. D **60**, 045003 (1999) doi:10.1103/PhysRevD.60.045003 [hep-th/9901109].
- [11] A. Bashir, A. Raya and J. Rodriguez-Quintero, Phys. Rev. D **88**, 054003 (2013) doi:10.1103/PhysRevD.88.054003 [arXiv:1302.5829 [hep-ph]].
- [12] M. Hopfer, C. S. Fischer and R. Alkofer, JHEP **1411**, 035 (2014) doi:10.1007/JHEP11(2014)035 [arXiv:1405.7031 [hep-ph]].
- [13] A. Doff and A. A. Natale, Phys. Rev. D **94**, no. 7, 076005 (2016) doi:10.1103/PhysRevD.94.076005 [arXiv:1610.02564 [hep-ph]].
- [14] D. Binosi, C. D. Roberts and J. Rodriguez-Quintero, Phys. Rev. D **95**, no. 11, 114009 (2017) doi:10.1103/PhysRevD.95.114009 [arXiv:1611.03523 [nucl-th]].
- [15] C. Bernard *et al.* [MILC Collaboration], Phys. Rev. D **71**, 034504 (2005) doi:10.1103/PhysRevD.71.034504 [hep-lat/0405029].
- [16] M. Cheng *et al.*, Phys. Rev. D **74**, 054507 (2006)

- doi:10.1103/PhysRevD.74.054507 [hep-lat/0608013].
- [17] Y. Aoki, S. Borsanyi, S. Durr, Z. Fodor, S. D. Katz, S. Krieg and K. K. Szabo, *JHEP* **0906**, 088 (2009) doi:10.1088/1126-6708/2009/06/088 [arXiv:0903.4155 [hep-lat]].
- [18] S. Borsanyi *et al.* [Wuppertal-Budapest Collaboration], *JHEP* **1009**, 073 (2010) doi:10.1007/JHEP09(2010)073 [arXiv:1005.3508 [hep-lat]].
- [19] A. Bazavov *et al.*, *Phys. Rev. D* **85**, 054503 (2012) doi:10.1103/PhysRevD.85.054503 [arXiv:1111.1710 [hep-lat]].
- [20] L. Levkova, *PoS LATTICE 2011*, 011 (2011) doi:10.22323/1.139.0011 [arXiv:1201.1516 [hep-lat]].
- [21] T. Bhattacharya *et al.*, *Phys. Rev. Lett.* **113**, no. 8, 082001 (2014) doi:10.1103/PhysRevLett.113.082001 [arXiv:1402.5175 [hep-lat]].
- [22] P. de Forcrand, J. Langelage, O. Philipsen and W. Unger, *Phys. Rev. Lett.* **113**, no. 15, 152002 (2014) doi:10.1103/PhysRevLett.113.152002 [arXiv:1406.4397 [hep-lat]].
- [23] A. Bazavov, H.-T. Ding, P. Hegde, F. Karsch, E. Laermann, S. Mukherjee, P. Petreczky and C. Schmidt, *Phys. Rev. D* **95**, no. 7, 074505 (2017) doi:10.1103/PhysRevD.95.074505 [arXiv:1701.03548 [hep-lat]].
- [24] S. x. Qin, L. Chang, H. Chen, Y. x. Liu and C. D. Roberts, *Phys. Rev. Lett.* **106**, 172301 (2011) doi:10.1103/PhysRevLett.106.172301 [arXiv:1011.2876 [nucl-th]].
- [25] C. S. Fischer, J. Luecker and J. A. Mueller, *Phys. Lett. B* **702**, 438 (2011) doi:10.1016/j.physletb.2011.07.039 [arXiv:1104.1564 [hep-ph]].
- [26] A. Ayala, A. Bashir, C. A. Dominguez, E. Gutierrez, M. Loewe and A. Raya, *Phys. Rev. D* **84**, 056004 (2011) doi:10.1103/PhysRevD.84.056004 [arXiv:1106.5155 [hep-ph]].
- [27] E. Gutierrez, A. Ahmad, A. Ayala, A. Bashir and A. Raya, *J. Phys. G* **41**, 075002 (2014) doi:10.1088/0954-3899/41/7/075002 [arXiv:1304.8065 [hep-ph]].
- [28] F. Gao, J. Chen, Y. X. Liu, S. X. Qin, C. D. Roberts and S. M. Schmidt, *Phys. Rev. D* **93**, no. 9, 094019 (2016) doi:10.1103/PhysRevD.93.094019 [arXiv:1507.00875 [nucl-th]].
- [29] G. Eichmann, C. S. Fischer and C. A. Welzbacher, *Phys. Rev. D* **93**, no. 3, 034013 (2016) doi:10.1103/PhysRevD.93.034013 [arXiv:1509.02082 [hep-ph]].
- [30] F. Gao and Y. x. Liu, *Phys. Rev. D* **94**, no. 7, 076009 (2016) doi:10.1103/PhysRevD.94.076009 [arXiv:1607.01675 [hep-ph]].
- [31] C. S. Fischer, *Prog. Part. Nucl. Phys.* **105**, 1 (2019) doi:10.1016/j.pnpnp.2019.01.002 [arXiv:1810.12938 [hep-ph]].
- [32] C. Shi, X. T. He, W. B. Jia, Q. W. Wang, S. S. Xu and H. S. Zong, *JHEP* **06**, 122 (2020) doi:10.1007/JHEP06(2020)122 [arXiv:2004.09918 [hep-ph]].
- [33] V. P. Gusynin, V. A. Miransky and I. A. Shovkovy, *Phys. Lett. B* **349**, 477 (1995) doi:10.1016/0370-2693(95)00232-A [hep-ph/9412257].
- [34] D. S. Lee, C. N. Leung and Y. J. Ng, *Phys. Rev. D* **55**, 6504 (1997) doi:10.1103/PhysRevD.55.6504 [hep-th/9701172].
- [35] D. K. Hong, *Phys. Rev. D* **57**, 3759 (1998) doi:10.1103/PhysRevD.57.3759 [hep-ph/9707432].
- [36] E. J. Ferrer and V. de la Incera, *Phys. Lett. B* **481**, 287 (2000) doi:10.1016/S0370-2693(00)00482-2 [hep-ph/0004113].
- [37] A. Ayala, A. Bashir, A. Raya and E. Rojas, *Phys. Rev. D* **73**, 105009 (2006) doi:10.1103/PhysRevD.73.105009 [hep-ph/0602209].
- [38] E. Rojas, A. Ayala, A. Bashir and A. Raya, *Phys. Rev. D* **77**, 093004 (2008) doi:10.1103/PhysRevD.77.093004 [arXiv:0803.4173 [hep-ph]].
- [39] A. Ayala, A. Bashir, E. Gutierrez, A. Raya and A. Sanchez, *Phys. Rev. D* **82**, 056011 (2010) doi:10.1103/PhysRevD.82.056011 [arXiv:1007.4249 [hep-ph]].
- [40] D. N. Kabat, K. M. Lee and E. J. Weinberg, *Phys. Rev. D* **66**, 014004 (2002) doi:10.1103/PhysRevD.66.014004 [hep-ph/0204120].
- [41] V. A. Miransky and I. A. Shovkovy, *Phys. Rev. D* **66**, 045006 (2002) doi:10.1103/PhysRevD.66.045006 [hep-ph/0205348].
- [42] M. D'Elia, S. Mukherjee and F. Sanfilippo, *Phys. Rev. D* **82**, 051501 (2010) doi:10.1103/PhysRevD.82.051501 [arXiv:1005.5365 [hep-lat]].
- [43] G. S. Bali, F. Bruckmann, G. Endrodi, Z. Fodor, S. D. Katz, S. Krieg, A. Schafer and K. K. Szabo, *JHEP* **1202**, 044 (2012) doi:10.1007/JHEP02(2012)044 [arXiv:1111.4956 [hep-lat]].
- [44] G. S. Bali, F. Bruckmann, G. Endrodi, Z. Fodor, S. D. Katz and A. Schafer, *Phys. Rev. D* **86**, 071502 (2012) doi:10.1103/PhysRevD.86.071502 [arXiv:1206.4205 [hep-lat]].
- [45] G. S. Bali, F. Bruckmann, G. Endrodi, F. Gruber and A. Schafer, *JHEP* **1304**, 130 (2013) doi:10.1007/JHEP04(2013)130 [arXiv:1303.1328 [hep-lat]].
- [46] V. G. Bornyakov, P. V. Buividovich, N. Cundy, O. A. Kochetkov and A. Schafer, *Phys. Rev. D* **90**, no. 3, 034501 (2014) doi:10.1103/PhysRevD.90.034501 [arXiv:1312.5628 [hep-lat]].
- [47] V. P. Pagura, D. Gomez Dumm, S. Noguera and N. N. Scoccola, *Phys. Rev. D* **95** (2017) no.3, 034013 doi:10.1103/PhysRevD.95.034013 [arXiv:1609.02025 [hep-ph]].
- [48] K. Fukushima and Y. Hidaka, *Phys. Rev. Lett.* **110**, no. 3, 031601 (2013) doi:10.1103/PhysRevLett.110.031601 [arXiv:1209.1319 [hep-ph]].
- [49] N. Mueller and J. M. Pawłowski, *Phys. Rev. D* **91**, no. 11, 116010 (2015) doi:10.1103/PhysRevD.91.116010 [arXiv:1502.08011 [hep-ph]].
- [50] L. X. Gutierrez-Guerrero, A. Bashir, I. C. Cloet and C. D. Roberts, *Phys. Rev. C* **81**, 065202 (2010) doi:10.1103/PhysRevC.81.065202 [arXiv:1002.1968 [nucl-th]].
- [51] H. L. L. Roberts, C. D. Roberts, A. Bashir, L. X. Gutierrez-Guerrero and P. C. Tandy, *Phys. Rev. C* **82**, 065202 (2010) doi:10.1103/PhysRevC.82.065202 [arXiv:1009.0067 [nucl-th]].
- [52] H. L. L. Roberts, A. Bashir, L. X. Gutierrez-Guerrero, C. D. Roberts and D. J. Wilson, *Phys. Rev. C* **83**, 065206 (2011) doi:10.1103/PhysRevC.83.065206 [arXiv:1102.4376 [nucl-th]].
- [53] C. Chen, L. Chang, C. D. Roberts, S. Wan and D. J. Wilson, *Few Body Syst.* **53**, 293 (2012) doi:10.1007/s00601-012-0466-3 [arXiv:1204.2553 [nucl-th]].

- [54] H. L. L. Roberts, L. Chang, I. C. Cloet and C. D. Roberts, *Few Body Syst.* **51**, 1 (2011) doi:10.1007/s00601-011-0225-x [arXiv:1101.4244 [nucl-th]].
- [55] M. A. Bedolla, J. J. Cobos-Martínez and A. Bashir, *Phys. Rev. D* **92**, no. 5, 054031 (2015) doi:10.1103/PhysRevD.92.054031 [arXiv:1601.05639 [hep-ph]].
- [56] M. A. Bedolla, K. Raya, J. J. Cobos-Martínez and A. Bashir, *Phys. Rev. D* **93**, no. 9, 094025 (2016) doi:10.1103/PhysRevD.93.094025 [arXiv:1606.03760 [hep-ph]].
- [57] K. Raya, M. A. Bedolla, J. J. Cobos-Martínez and A. Bashir, *Few Body Syst.* **59**, no. 6, 133 (2018) doi:10.1007/s00601-018-1455-y [arXiv:1711.00383 [nucl-th]].
- [58] L. X. Gutiérrez-Guerrero, A. Bashir, M. A. Bedolla and E. Santopinto, *Phys. Rev. D* **100**, no.11, 114032 (2019) doi:10.1103/PhysRevD.100.114032 [arXiv:1911.09213 [nucl-th]].
- [59] P. O. Bowman, U. M. Heller, D. B. Leinweber, M. B. Parappilly and A. G. Williams, *Phys. Rev. D* **70**, 034509 (2004) doi:10.1103/PhysRevD.70.034509 [hep-lat/0402032].
- [60] D. Dudal, J. A. Gracey, S. P. Sorella, N. Vandersickel and H. Verschelde, *Phys. Rev. D* **78** (2008) 065047 doi:10.1103/PhysRevD.78.065047 [arXiv:0806.4348 [hep-th]].
- [61] M. Q. Huber, R. Alkofer and S. P. Sorella, *AIP Conf. Proc.* **1343**, 158 (2011) doi:10.1063/1.3574962 [arXiv:1010.4802 [hep-th]].
- [62] P. Boucaud, J. P. Leroy, A. L. Yaouanc, J. Micheli, O. Pene and J. Rodriguez-Quintero, *Few Body Syst.* **53**, 387 (2012) doi:10.1007/s00601-011-0301-2 [arXiv:1109.1936 [hep-ph]].
- [63] A. Ayala, A. Bashir, D. Binosi, M. Cristoforetti and J. Rodriguez-Quintero, *Phys. Rev. D* **86**, 074512 (2012) doi:10.1103/PhysRevD.86.074512 [arXiv:1208.0795 [hep-ph]].
- [64] A. Ahmad and A. Raya, *J. Phys. G* **43**, no. 6, 065002 (2016) doi:10.1088/0954-3899/43/6/065002 [arXiv:1602.06448 [hep-ph]].
- [65] F. Gao, S. X. Qin, C. D. Roberts and J. Rodriguez-Quintero, *Phys. Rev. D* **97** (2018) no.3, 034010 doi:10.1103/PhysRevD.97.034010 [arXiv:1706.04681 [hep-ph]].
- [66] D. Ebert, T. Feldmann and H. Reinhardt, *Phys. Lett. B* **388**, 154 (1996) doi:10.1016/0370-2693(96)01158-6 [hep-ph/9608223].
- [67] C. D. Roberts, *Prog. Part. Nucl. Phys.* **61**, 50 (2008) doi:10.1016/j.ppnp.2007.12.034 [arXiv:0712.0633 [nucl-th]].
- [68] F. Marquez, A. Ahmad, M. Buballa and A. Raya, *Phys. Lett. B* **747**, 529 (2015) doi:10.1016/j.physletb.2015.06.031 [arXiv:1504.06730 [nucl-th]].
- [69] Z. F. Cui, Y. L. Du and H. S. Zong, *Int. J. Mod. Phys. Conf. Ser.* **29**, 1460232 (2014). doi:10.1142/S2010194514602324
- [70] K. I. Wang, Y. x. Liu, L. Chang, C. D. Roberts and S. M. Schmidt, *Phys. Rev. D* **87**, no. 7, 074038 (2013) doi:10.1103/PhysRevD.87.074038 [arXiv:1301.6762 [nucl-th]].
- [71] J. S. Schwinger, *Phys. Rev.* **82**, 664 (1951). doi:10.1103/PhysRev.82.664
- [72] V. Fock, *Phys. Z. Sowjetunion* **12**, 404 (1937).
- [73] M. Ferreira, P. Costa, O. Loureno, T. Frederico and C. Providencia, *Phys. Rev. D* **89**, no.11, 116011 (2014) doi:10.1103/PhysRevD.89.116011 [arXiv:1404.5577 [hep-ph]].
- [74] R. L. S. Farias, K. P. Gomes, G. I. Krein and M. B. Pinto, *Phys. Rev. C* **90**, no.2, 025203 (2014) doi:10.1103/PhysRevC.90.025203 [arXiv:1404.3931 [hep-ph]].
- [75] R. L. S. Farias, V. S. Timoteo, S. S. Avancini, M. B. Pinto and G. Krein, *Eur. Phys. J. A* **53**, no.5, 101 (2017) doi:10.1140/epja/i2017-12320-8 [arXiv:1603.03847 [hep-ph]].